Double-quantum filtered ^{23}Na NMR and MRI: Selective detection of ordered sodium in an inhomogeneous B_0 field

Stephen Wimperis [a],[*],[1], Galina E. Pavlovskaya [b]

[a] *Department of Chemistry, Faraday Building, Lancaster University, Lancaster LA1 4YB, United Kingdom*
[b] *Sir Peter Mansfield Imaging Centre, University of Nottingham, University Park, Nottingham NG7 2RD, United Kingdom*

ARTICLE INFO

ABSTRACT

Double-quantum filtered ^{23}Na NMR experiments with one or two "magic angle" (54.7°) pulses in the filter step are widely used for selective observation of sodium ions that are interacting with ordered biological structures ("ordered sodium") and hence exhibit a distribution of quadrupolar splittings in their NMR spectrum. This approach has recently been extended to ^{23}Na MRI where the conventional experiment has been modified, omitting the 180° pulse to reduce the absorption of radiofrequency energy during human studies. Here, the "magic angle" double-quantum filtered ^{23}Na NMR experiment (without a 180° pulse) is analysed in terms of coherence pathways that lead to refocusing in an inhomogeneous B_0 field ("echoes") and those that do not ("antiechoes"). It is shown that the echo and antiecho pathways can be separated by phase cycling and that the antiecho pathway contributes very little to the overall signal in an inhomogeneous B_0 field. Hence, a double-quantum filtered ^{23}Na NMR experiment that utilises just the echo pathway and so achieves complete refocusing of the effects of B_0 inhomogeneity without making use of a 180° pulse is proposed. The new method is demonstrated both in ^{23}Na NMR spectroscopy in an inhomogeneous B_0 field and in ^{23}Na MRI of a three-component phantom.

1. Introduction

Multiple-quantum and multiple-quantum filtration NMR techniques have become essential tools in the study of spin I = 3/2 nuclei, such as ^{7}Li, ^{11}B, ^{23}Na, ^{39}K, ^{87}Rb and ^{131}Xe [1–5]. For example, in purely isotropic liquids or biological systems, triple-quantum filtered ^{23}Na NMR can be used to separate the signal from sodium ions experiencing slow dynamics (and hence exhibiting biexponential spin relaxation) from those experiencing very fast dynamics (and so exhibiting monoexponential spin relaxation) [3]. Furthermore, in these systems triple-quantum filtered NMR can assist in the accurate measurement of biexponential I = 3/2 spin relaxation rate constants [3,6]. In most heterogeneous biological systems a further, non-isotropic ion environment is encountered, where the sodium ions interact with ordered molecular structures ("ordered sodium") and hence exhibit a distribution of quadrupolar splittings in their ^{23}Na NMR spectrum [7,8]. This pool of ordered ions can be selectively detected using a double-quantum filtration NMR technique where one or more of the radiofrequency pulses in the filtration step have a 54.7° (or "magic angle") flip angle [3,7,8].

In addition to their wide application in NMR spectroscopy, multiple-quantum and multiple-quantum filtration techniques have also been used in ^{23}Na MRI with the aim of obtaining a novel source of image contrast [9–28]. In early demonstrations, many of the proposed methods used the same radiofrequency pulse sequences applied in NMR spectroscopy, with a 180° pulse in the centre of the evolution period (that preceding the multiple-quantum filter) to refocus the effects of B_0 inhomogeneity during that period [9–11,13,15,25]. More recently, concerns over the specific absorption rate (SAR) of radiofrequency energy during human ^{23}Na MRI studies has led to an interest in methods where this 180° pulse is omitted so as to reduce the SAR. Pulse techniques that do not use a 180° refocusing pulse have been applied both in triple-quantum filtered ^{23}Na MRI [12,14,16–24,28] and also, more recently still, in "magic angle" double-quantum filtered ^{23}Na MRI [26,27] where the aim is to selectively image sodium ions in ordered environments. However, there has been an awareness that the absence of the 180° pulse may increase the susceptibility of some multiple-quantum filtered ^{23}Na MRI experiments to the effects of B_0 inhomogeneity.

In this work we analyse the "magic angle" double-quantum filtered

^{23}Na NMR experiment (without a 180° pulse) in terms of coherence pathways that lead to refocusing in an inhomogeneous B_0 field ("echoes") and those that do not ("antiechoes") [29]. We show that the echo and antiecho pathways can be separated by phase cycling [29] and that the antiecho pathway contributes very little to the overall signal in an inhomogeneous B_0 field. This leads us to propose and demonstrate a double-quantum filtered [23]Na MRI experiment that utilises just the echo pathway and so achieves complete refocusing of the effects of B_0 inhomogeneity without making use of a 180° pulse. This method is based on principles used in a previously proposed triple-quantum filtered [23]Na MRI experiment that fully refocuses the effects of B_0 inhomogeneity [12,14], which itself is related to a method used in ^{23}Na NMR spectroscopy *in vivo* for forming spin echoes without use of a 180° pulse [30,31], and in related methods [16–24,28].

For a recent overview of the wider aspects of [23]Na MRI, we direct the interested reader to the review by Gast et al. [32].

2. Theory

2.1. Multiple-quantum filtered ^{23}Na (I = 3/2) NMR

Following the original work of Jaccard et al. [3], the spin I = 3/2 density operator is most conveniently expanded as a linear combination of spherical tensor operators of rank l and coherence order p:

$$\sigma(t) = \sum_{l=0}^{2I} \sum_{p=-l}^{l} b_{l,p}(t) T_{l,p} \tag{1}$$

An initial 90°$_y$ pulse yields the density operator

$$\sigma(\tau = 0) = T_{1,-1} - T_{1,+1} \tag{2}$$

where, as usual, we have omitted several constants (number of spins, gyromagnetic ratio, temperature, etc.). If this density operator then evolves purely under the influence of biexponential quadrupolar transverse relaxation for a time τ, the result can be written [3]

$$\sigma(\tau) = f_{11}(\tau)\left(T_{1,-1} - T_{1,+1}\right) + f_{31}(\tau)\left(T_{3,-1} - T_{3,+1}\right) \tag{3}$$

with the transverse relaxation functions

$$f_{11}(t) = \frac{1}{5}\left(3\exp\{-R_{fast}t\} + 2\exp\{-R_{slow}t\}\right) \tag{4a}$$

$$f_{31}(t) = \frac{\sqrt{6}}{5}\left(\exp\{-R_{fast}t\} - \exp\{-R_{slow}t\}\right) \tag{4b}$$

The rate constants R_{fast} and R_{slow} describe the two components of the biexponential relaxation. These are equal if the modulation of the [23]Na quadrupolar interaction is fast compared with the Larmor frequency ω_0 and so in this case $f_{31}(\tau) \approx 0$ and no third-rank ($l = 3$) coherences develop. However, for the more general case, where the modulation of the quadrupolar interaction is slower, $R_{fast} > R_{slow}$ and $f_{31}(\tau) \neq 0$. A further radiofrequency pulse of flip angle β and phase ϕ changes the coherence order (but not the rank) according to

$$T_{l,p} \xrightarrow{\beta\left(I_y\cos\phi - I_x\sin\phi\right)} \sum_{p'=-l}^{l} T_{l,p'} \, d_{p',p}^{l}(\beta)\exp\{-i\Delta p\phi\} \tag{5}$$

where $d_{p',p}^{l}(\beta)$ is a reduced Wigner rotation matrix element (tabulated in many places, e.g., Ref. [33]) and $\Delta p = p' - p$ is the change in coherence order under the pulse, with p' being the new coherence order. In particular, a 90°$_x$ ($\phi = -90°$) pulse applied to the density operator in Eq. (3) will create the triple-quantum state

$$\sigma'(\tau) = -\frac{\sqrt{15}}{4}f_{31}(\tau)(T_{3,-3} - T_{3,+3}) \tag{6}$$

Tensor operators of other coherence orders will also be created but the contribution of these to the final NMR signal can be cancelled by using phase cycling [29], which is an essential component of the multiple-quantum filter (and implicitly assumed in this calculation). Finally, a further 90°$_x$ pulse will convert the triple-quantum coherences back into observable single-quantum coherences, which by convention have coherence order p = −1 if quadrature detection is used:

$$\sigma''(\tau) = \frac{15}{16}f_{31}(\tau)T_{3,-1} \tag{7}$$

This final signal will only be nonzero if $f_{31}(\tau) \neq 0$, hence this triple-quantum filtered experiment can be used to separate the NMR signal of sodium ions experiencing slow dynamics (and hence exhibiting biexponential spin relaxation) from that of ions experiencing very fast dynamics [3,6].

In contrast, if the density operator in Eq. (2) evolves purely under the influence of a resolved spin I = 3/2 quadrupolar splitting $2\omega_Q$ for a time τ, the result can be written [3,8]

$$\sigma(\tau) = g_{11}(\tau)\left(T_{1,-1} - T_{1,+1}\right) + g_{21}(\tau)\left(T_{2,-1} + T_{2,+1}\right) + g_{31}(\tau)\left(T_{3,-1} - T_{3,+1}\right) \tag{8}$$

with

$$g_{11}(t) = (1/5)\{2 + 3\cos(2\omega_Q t)\} \tag{9a}$$

$$g_{21}(t) = i\sqrt{(3/5)}\sin(2\omega_Q t) \tag{9b}$$

$$g_{31}(t) = -(\sqrt{6}/5)\{1 - \cos(2\omega_Q t)\} \tag{9c}$$

Hence a significant difference between evolution as a result of biexponential relaxation, Eqs. (3) and (4), or of residual quadrupolar splittings, Eqs. (8) and (9), is that only in the latter case do rank $l = 2$ tensors, $T_{2,\pm1}$, appear and this forms the basis of a method of distinguishing the two effects [3,7,8]. A β_y ($\phi = 0°$) pulse applied to the density operator in Eq. (8) will create the double-quantum state

$$\sigma'(\tau) = g_{21}(\tau)\left(T_{2,-2} - T_{2,+2}\right)\sin\beta - \frac{\sqrt{10}}{4}g_{31}(\tau)\left(T_{3,-2} + T_{3,+2}\right)\sin\beta\left(1 - 3\cos^2\beta\right) \tag{10}$$

and again the contribution of only these operators to the final NMR signal can be selected using phase cycling. However, the presence of rank $l = 3$ tensors in Eq. (10) shows that double-quantum filtration alone is not sufficient to select for only sodium ions exhibiting quadrupolar splittings since rank $l = 3$ double-quantum coherences, $T_{3,\pm2}$, will also be excited from the relaxation-only density operator in Eq. (3). Finally, a β'_y pulse will convert the double-quantum coherences back into observable (p = −1) single-quantum coherences:

$$\sigma''(\tau) = -g_{21}(\tau)T_{2,-1}\sin\beta\sin\beta' - \frac{5}{8}g_{31}(\tau)\,T_{3,-1}\sin\beta\left(1 - 3\cos^2\beta\right)\sin\beta'\left(1 - 3\cos^2\beta'\right) \tag{11}$$

Now it can be seen, following Jaccard et al. [3] and Eliav et al. [7], that if either or both of the flip angles β or β' in the double-quantum filter is set to the "magic angle" $\arccos(1/\sqrt{3}) = 54.7°$ (the root of $1 - 3\cos^2\beta = 0$) then third-rank coherences are suppressed and only second-rank coherences will appear. Thus, the resulting spectrum will arise from only those [23]Na nuclei that exhibit a residual quadrupolar splitting. With $\beta = \beta' = 54.7°$ the density operator at the start of the acquisition period becomes

$$\sigma''(\tau) = -\frac{2}{3}g_{21}(\tau)T_{2,-1} \tag{12}$$

while if either $\beta = 90°$ and $\beta' = 54.7°$ or $\beta = 54.7°$ and $\beta' = 90°$ it becomes

$$\sigma''(\tau) = -\frac{\sqrt{2}}{\sqrt{3}} g_{21}(\tau) \, T_{2,-1} \tag{13}$$

2.2. "Magic angle" double-quantum filtered ^{23}Na (I = 3/2) NMR without a 180° pulse

Fig. 1 compares the pulse sequences for "magic angle" double-quantum filtration with (Fig. 1a) and without (Fig. 1b) the 180° refocusing pulse in the evolution period. In the sequence in Fig. 1a, the 180° pulse removes the effects of any resonance offsets, including those introduced by B_0 inhomogeneity, during the evolution period τ. A suitable phase cycle for the pulse sequence in Fig. 1a is given in Table 1.

The pulse sequence in Fig. 1b is best analysed by considering the p = +1 (blue or "echo") pathway and the p = −1 (red or "antiecho") pathway in the evolution period separately. If the initial density operator in Eq. (2) evolves under the influence of a resolved spin I = 3/2 quadrupolar splitting $2\omega_Q$ *and* under a resonance offset Ω (representing either an instrumental offset or the effects of B_0 inhomogeneity) for a time τ we find

$$\sigma_{\text{echo}}(\tau) = \left\{ -g_{11}(\tau) \, T_{1,+1} + g_{21}(\tau) \, T_{2,+1} - g_{31}(\tau) \, T_{3,+1} \right\} \exp\{-i\Omega\tau\} \tag{14}$$

$$\sigma_{\text{antiecho}}(\tau) = \left\{ +g_{11}(\tau) \, T_{1,-1} + g_{21}(\tau) \, T_{2,-1} + g_{31}(\tau) \, T_{3,-1} \right\} \exp\{+i\Omega\tau\} \tag{15}$$

A β_y ($\phi = 0°$) pulse applied to these density operators will create the double-quantum states

$$\sigma'_{\text{echo}}(\tau) = g_{21}(\tau) \left\{ T_{2,-2} \, d^2_{-2,+1}(\beta) + T_{2,+2} \, d^2_{+2,+1}(\beta) \right\} \exp\{-i\Omega\tau\}$$
$$- g_{31}(\tau) \left\{ T_{3,-2} \, d^3_{-2,+1}(\beta) + T_{3,+2} \, d^3_{+2,+1}(\beta) \right\} \exp\{-i\Omega\tau\} \tag{16a}$$

$$\sigma'_{\text{antiecho}}(\tau) = g_{21}(\tau) \left\{ T_{2,-2} \, d^2_{-2,-1}(\beta) + T_{2,+2} \, d^2_{+2,-1}(\beta) \right\} \exp\{+i\Omega\tau\}$$
$$+ g_{31}(\tau) \left\{ T_{3,-2} \, d^3_{-2,-1}(\beta) + T_{3,+2} \, d^3_{+2,-1}(\beta) \right\} \exp\{+i\Omega\tau\} \tag{16b}$$

and again phase cycling is used to select only these contributions to the final signal. We will now assume that the free precession period Δ between the two filter pulses has negligible duration (this topic will be discussed further below) and continue the calculation by applying a β'_y ($\phi = 0°$) pulse to create the observable (p = −1) single-quantum coherences:

$$\sigma''_{\text{echo}}(\tau) = g_{21}(\tau) \, T_{2,-1} \left\{ d^2_{-2,+1}(\beta) \, d^2_{-1,-2}(\beta') + d^2_{+2,+1}(\beta) \, d^2_{-1,+2}(\beta') \right\} \exp\{-i\Omega\tau\}$$
$$- g_{31}(\tau) \, T_{3,-1} \left\{ d^3_{-2,+1}(\beta) \, d^3_{-1,-2}(\beta') + d^3_{+2,+1}(\beta) d^3_{-1,+2}(\beta') \right\} \exp\{-i\Omega\tau\} \tag{17a}$$

$$\sigma''_{\text{antiecho}}(\tau) = g_{21}(\tau) \, T_{2,-1} \left\{ d^2_{-2,-1}(\beta) \, d^2_{-1,-2}(\beta') + d^2_{+2,-1}(\beta) \, d^2_{-1,+2}(\beta') \right\} \exp\{+i\Omega\tau\}$$
$$+ g_{31}(\tau) \, T_{3,-1} \left\{ d^3_{-2,-1}(\beta) \, d^3_{-1,-2}(\beta') + d^3_{+2,-1}(\beta) \, d^3_{-1,+2}(\beta') \right\} \exp\{+i\Omega\tau\} \tag{17b}$$

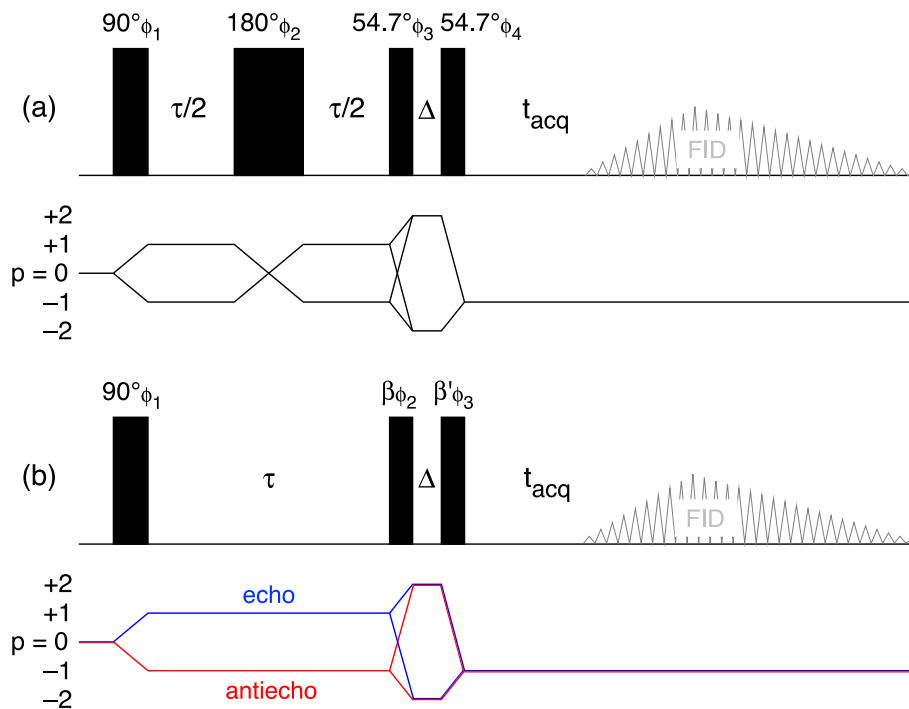**Fig. 1.** Pulse sequences and coherence pathways for spin I = 3/2 "magic angle" double-quantum filtration with (a) and without (b) the 180° refocusing pulse in the evolution period τ. The experiment in (b) can be performed either with retention of both the echo (blue) and antiecho (red) coherence pathways or with retention of just one of the two pathways. Suitable phase cycles for these sequences are given in Table 1.

Table 1

Phase cycles for the pulse sequences in Figs. 1 and 2.

These phase cycles will select the coherence pathways shown in Figs. 1 and 2 and are the ones used in our experiments. (Note that many equivalent schemes will exist.)

Pulse sequence in Fig. 1a

$\phi_1 = 0°\ 90°\ 180°\ 270°\ 180°\ 270°\ 0°\ 90°$

$\phi_2 = 0°\ 90°\ 180°\ 270°\ 0°\ 90°\ 180°\ 270°\ 90°\ 180°\ 270°\ 0°\ 90°\ 180°\ 270°\ 0°$
      $180°\ 270°\ 0°\ 90°\ 180°\ 270°\ 0°\ 90°\ 270°\ 0°\ 90°\ 180°\ 270°\ 0°\ 90°\ 180°$

$\phi_3 = 0°\ 90°\ 180°\ 270°$

$\phi_4 = 0°$

$\phi_{Rx} = 0°\ 180°\ 0°\ 180°\ 180°\ 0°\ 180°\ 0°\ 180°\ 0°\ 180°\ 0°\ 0°\ 180°\ 0°\ 180°$

Pulse sequence in Fig. 1b with retention of both echo and antiecho pathways

$\phi_1 = 0°\ 90°\ 180°\ 270°\ 180°\ 270°\ 0°\ 90°$

$\phi_2 = 0°\ 90°\ 180°\ 270°$

$\phi_3 = 0°$

$\phi_{Rx} = 0°\ 180°\ 0°\ 180°\ 180°\ 0°\ 180°\ 0°$

Pulse sequence in Fig. 1b and Fig. 2c with echo selection (blue pathway)*

$\phi_1 = 0°$

$\phi_2 = 0°\ 0°\ 0°\ 0°\ 90°\ 90°\ 90°\ 90°\ 180°\ 180°\ 180°\ 180°\ 270°\ 270°\ 270°\ 270°$

$\phi_3 = 0°\ 90°\ 180°\ 270°\ 90°\ 180°\ 270°\ 0°\ 180°\ 270°\ 0°\ 90°\ 270°\ 0°\ 90°\ 180°$

$\phi_{Rx} = 0°\ 270°\ 180°\ 90°\ 180°\ 90°\ 0°\ 270°$

Pulse sequence in Fig. 1b with antiecho selection (red pathway)*

$\phi_1 = 0°$

$\phi_2 = 0°\ 0°\ 0°\ 0°\ 90°\ 90°\ 90°\ 90°\ 180°\ 180°\ 180°\ 180°\ 270°\ 270°\ 270°\ 270°$

$\phi_3 = 0°\ 90°\ 180°\ 270°\ 90°\ 180°\ 270°\ 0°\ 180°\ 270°\ 0°\ 90°\ 270°\ 0°\ 90°\ 180°$

$\phi_{Rx} = 0°\ 270°\ 180°\ 90°$

Spin-echo pulse sequence in Fig. 2a

$\phi_1 = 0°$

$\phi_2 = 0°\ 90°\ 180°\ 270°$

$\phi_{Rx} = 0°\ 180°$

Triple-quantum filtered echo in Fig. 2b

$\phi_1 = 0°\ 60°\ 120°\ 180°\ 240°\ 300°\ 240°\ 300°\ 0°\ 60°\ 120°\ 180°\ 120°\ 180°\ 240°\ 300°\ 0°\ 60°$

$\phi_2 = 0°\ 60°\ 120°\ 180°\ 240°\ 300°\ 120°\ 180°\ 240°\ 300°\ 0°\ 60°\ 240°\ 300°\ 0°\ 60°\ 120°\ 180°$

$\phi_3 = 0°\ 0°\ 0°\ 0°\ 0°\ 0°\ 120°\ 120°\ 120°\ 120°\ 120°\ 120°\ 240°\ 240°\ 240°\ 240°\ 240°\ 240°$

$\phi_{Rx} = 0°\ 180°$

* Note that if the free induction decays are stored appropriately, the echo signal (blue pathway in Fig. 1b and 2c) and antiecho signal (red pathway in Fig. 1b) can be calculated from the same data set as only the receiver phase differs between the two experiments.

If $\beta = \beta' = 54.7°$ then Eq. (17) becomes

$$\sigma''_{echo}(\tau) = -\frac{2}{9}g_{21}(\tau)\,T_{2,-1}\exp\{-i\Omega\tau\} + \frac{5}{18}g_{31}(\tau)\,T_{3,-1}\exp\{-i\Omega\tau\} \quad (18a)$$

$$\sigma''_{antiecho}(\tau) = -\frac{4}{9}g_{21}(\tau)\,T_{2,-1}\exp\{+i\Omega\tau\} - \frac{5}{18}g_{31}(\tau)\,T_{3,-1}\exp\{+i\Omega\tau\} \quad (18b)$$

Conventionally, the experiment in Fig. 1b has been recorded while retaining both the echo and antiecho signals in the evolution period, which requires no additional phase cycling as the evolution of the density operator as a function of τ is inherently amplitude modulated. In this case the density operator at the start of acquisition is

$$\sigma''(\tau) = \sigma''_{echo}(\tau) + \sigma''_{antiecho}(\tau)$$
$$= -\frac{2}{3}g_{21}(\tau)\,T_{2,-1}\cos(\Omega\tau) - \frac{5i}{9}g_{31}(\tau)\,T_{3,-1}\sin(\Omega\tau) \quad (19)$$

Hence, as demonstrated in the very elegant paper by Gast et al. [27], rank $l = 3$ tensors are *not* suppressed in this experiment, unless $\Omega = 0$. This is an unrealisable condition in the presence of even a small degree of B_0 inhomogeneity and so this experiment does not successfully select exclusively for sodium ions exhibiting quadrupolar splittings.

However, as also shown by Gast et al. [27], if either of the flip angle combinations $\beta = 90°$ and $\beta' = 54.7°$ or $\beta = 54.7°$ and $\beta' = 90°$ are used then Eq. (17) becomes

$$\sigma''_{echo}(\tau) = -\frac{1}{\sqrt{6}}g_{21}(\tau)\,T_{2,-1}\exp\{-i\Omega\tau\} \quad (20a)$$

$$\sigma''_{antiecho}(\tau) = -\frac{1}{\sqrt{6}}g_{21}(\tau)\,T_{2,-1}\exp\{+i\Omega\tau\} \quad (20b)$$

and the sum is

$$\sigma''(\tau) = \sigma''_{echo}(\tau) + \sigma''_{antiecho}(\tau) = -\frac{\sqrt{2}}{\sqrt{3}}g_{21}(\tau)\,T_{2,-1}\cos(\Omega\tau) \quad (21)$$

In this case rank $l = 3$ tensors are fully suppressed, even when $\Omega \neq 0$, and so this experiment does successfully select for only sodium ions exhibiting quadrupolar splittings. A suitable phase cycle for the pulse sequence in Fig. 1b with retention of both echo and antiecho pathways is given in Table 1.

[In an apparent contradiction of the results above, where there is full suppression of rank $l = 3$ operators at all resonance offsets, Fig. 3 of Gast et al. [27] shows a small amplitude of rank $l = 3$ signal leaking through the double-quantum filter away from exact resonance when either $\beta = 90°$ and $\beta' = 54.7°$ or $\beta = 54.7°$ and $\beta' = 90°$. The reason for this is the inclusion of a significant delay between the two filter pulses (our Δ) of 50 μs in the calculations for Fig. 3 in Ref. [27], whereas we have assumed a negligible value for Δ above. In experimental practice over the last 40 years on a wide variety of instrumentation, one of us has been using a Δ of 2 or 3 μs in multiple-quantum and similar filters without ever encountering any problems. The purpose of this delay is simply to

allow the radiofrequency pulse phase to switch and this occurs on a sub-microsecond timescale. With $\Delta = 2\ \mu s$ and an offset $\Omega/2\pi = 100$ Hz, cos $(\Omega\Delta) = 0.9999992$ and $\sin(\Omega\Delta) = 0.0012566$, indicating negligible net precession. We can see no justification for using a longer free precession period within the multiple-quantum filter, especially as it only affects the experiment adversely.]

It is instructive to continue the density operator calculation for $\sigma''_{echo}(\tau)$ and $\sigma''_{antiecho}(\tau)$ in Eq. (20) into the acquisition period t_{acq}. During this period $T_{2,-1}$ has to evolve into in-phase $T_{1,-1}$ (which is the only component that induces signal in the receiver) under the influence of the quadrupolar splitting while at the same time still evolving under the resonance offset Ω:

$$\sigma''_{echo}(\tau, t_{acq}) = -\frac{1}{\sqrt{6}}g_{21}(\tau)\,g_{12}(t_{acq})\,T_{1,-1}\exp\{-i\Omega\tau\}\exp\{+i\Omega t_{acq}\}$$

$$(22a)$$

$$\sigma''_{antiecho}(\tau, t_{acq}) = -\frac{1}{\sqrt{6}}g_{21}(\tau)\,g_{12}(t_{acq})\,T_{1,-1}\exp\{+i\Omega\tau\}\exp\{+i\Omega t_{acq}\}$$

$$(22b)$$

where $g_{12}(t) = g_{21}(t)$ and we have retained only the observable $T_{1,-1}$ tensors. Inspection of Eq. (22a) shows that when $t_{acq} = \tau$ the exponential phase factors cancel each other, i.e., $\exp\{-i\Omega\tau\}\exp\{+i\Omega t_{acq}\} = 1$, for all values of Ω. In other words, a spin echo forms in the acquisition period (after a time τ) exactly as it would if the two pulses of the multiple-quantum filter were replaced by a single 180° pulse. This spin echo is a consequence of the coherence order changing sign from p = +1 in the evolution period to p = −1 in the acquisition period (as it does in a conventional spin-echo experiment). In contrast, Eq. (22b) shows that the so-called antiecho component of the signal does *not* generate a spin echo during acquisition: dephasing of the signal due to a spread of Ω values (i.e., B$_0$ inhomogeneity) in the evolution period τ continues unabated in the acquisition period t_{acq}. As a result, if the experiment of Fig. 1b (with retention of both pathways) is performed in an inhomogeneous B$_0$ field, the antiecho pathway will contribute very little to the overall signal. By the time that $T_{2,-1}$ has evolved into observable $T_{1,-1}$ under the influence of the quadrupolar splittings (typically a few milliseconds), the antiecho component of the signal will have dephased in the inhomogeneous B$_0$ field.

[In addition to the echo and antiecho arising from B$_0$ inhomogeneity, if there is a distribution of $2\omega_Q$ values, as seems certain in any heterogeneous biological tissue, then the product $g_{21}(\tau)g_{12}(t_{acq})$ in Eq. (22) will also give rise to *quadrupolar* echo and antiecho phenomena. This can be seen by expanding the sine term in Eq. (9b) into exponential form, with the echo also forming when $t_{acq} = \tau$. However, crucially, these quadrupolar echoes and antiechoes do not depend on the sign of the coherence order [34]; the product $g_{21}(\tau)g_{12}(t_{acq})$ occurs identically in both Eqs. (22a) and (22b). Hence, as we can also realistically rule out a spatial correlation between the B$_0$ field inhomogeneity and the distribution of quadrupolar splittings, the two effects can be treated separately and our arguments above about echoes and antiechoes in an inhomogeneous B$_0$ field are unaffected.]

2.3. "Magic angle" double-quantum filtered ^{23}Na (I = 3/2) NMR with echo selection

Phase cycling [29] can be used to select the echo and antiecho pathways separately in the experiment in Fig. 1b, just as it can be used to select the coherences in a multiple-quantum filter. Suitable 16-step phase cycles for the two (now) separate experiments are given in Table 1. These consist of four steps to select double-quantum coherences after the second pulse nested with four steps to select $\Delta p = -2$ (the echo pathway) or $\Delta p = 0$ (the antiecho pathway) over the two filter pulses. When used to select the echo pathway, this second 4-step phase cycle is sometimes known as Exorcycle [35]. A 3-step alternative exists that

utilises 120° phase increments [29]. The double-quantum filtered echo and antiecho methods will be demonstrated as two separate experiments below.

From the discussion above, it would seem that a double-quantum filtered ^{23}Na NMR experiment with echo selection has potentially much to recommend it in practice. It does not utilise a 180° pulse and so will have a lower SAR than the experiment in Fig. 1a. And yet, as long as there is negligible free precession during the Δ delay, in an inhomogeneous B$_0$ field an echo is formed in the acquisition period exactly the same as in a conventional spin-echo experiment. There will be no unwanted interference with this echo from the (weaker) antiecho signal because the latter has been fully suppressed by the additional phase cycling. These features of the double-quantum filtered echo experiment will be demonstrated experimentally below.

Selection of the echo pathway also means that the double-quantum filtered echo pulse sequence can be turned into a ^{23}Na MRI experiment in the same manner as for a simple $90° - \tau - 180°$ spin echo, with phase encoding gradients applied during the τ period after the initial 90° pulse and readout gradients applied both before and after the refocusing element [12,14]. Fig. 2 shows three pulse sequences for ^{23}Na (I = 3/2) MRI that will be used in the experimental work below, with the gradient scheme (common to all three pulse sequences) shown at the bottom. The conventional spin echo MRI sequence is shown in Fig. 2a, a previously demonstrated triple-quantum filtered echo MRI sequence is shown in Fig. 2b [12,14], and the double-quantum filtered echo MRI sequence proposed here is shown in Fig. 2c. All three MRI experiments utilise the echo coherence pathway and so will achieve full refocusing of the effects of B$_0$ inhomogeneity if performed with the correct timings.

Finally, it is worth noting the flip angle dependence of the unwanted rank $l = 3$ tensor operators in the double-quantum filtered echo experiment. This can be extracted from Eq. (17a) as

$$d^3_{-2,+1}(\beta)\,d^3_{-1,-2}(\beta') + d^3_{+2,+1}(\beta)\,d^3_{-1,+2}(\beta')$$
$$= \frac{5}{16}\sin\beta\sin\beta'\left(3\left(3\cos^2\beta' - 1\right)\cos^2\beta - 4\cos\beta\cos\beta' - 3\cos^2\beta' + 1\right)\quad(23)$$

As mentioned above, this term is zero if either $\beta = 90°$ and $\beta' = 54.7°$ or $\beta = 54.7°$ and $\beta' = 90°$, in which case Eq. (17a) reduces to Eq. (20a). However, considering the echo experiment on its own, it can be seen that there is a continuum of pairs of flip angles $\{\beta, \beta'\}$ that will result in the rank $l = 3$ terms being zero. For example, with $\beta = \beta' = \arccos(1/3) = 70.5°$, Eq. (17a) becomes

$$\sigma''_{echo}(\tau) = -\frac{32}{81}g_{21}(\tau)\,T_{2,-1}\exp\{-i\Omega\tau\}\quad(24)$$

Note, however, that the combination $\beta = \beta' = 70.5°$ does not zero the rank $l = 3$ term in the antiecho expression in Eq. (17b).

3. Experimental details

^{23}Na NMR and MRI experiments were performed at a Larmor frequency of $\omega_0/2\pi = 105.8$ MHz on a Bruker Avance III spectrometer and microimaging system, equipped with a vertical widebore 9.4 T magnet, micro2.5 imaging gradients, and a 25-mm dual-tuned ^{1}H/^{23}Na birdcage coil (WB40 probehead). All pulse sequences were home-written in TopSpin 3.6. Further details of the experimental NMR work can be found in the text and figure captions.

For ^{23}Na NMR spectroscopy the sample was 3% (w/v) xanthan gum in 150 mM NaCl(aq) contained in a 10-mm glass NMR tube. The xanthan gum polymer produces a non-isotropic average sodium ion environment and hence the ^{23}Na NMR spectrum exhibits a distribution of quadrupolar splittings, as evidenced by a non-zero signal in the "magic-angle" double-quantum filtered NMR experiment in Fig. 1a. The optimum evolution period τ in this experiment, indicating the maximum in the build-up of $T_{2,\pm1}$ coherences, was determined as being 4.5 ms.

For ^{23}Na MRI a phantom was constructed consisting of the above 10-
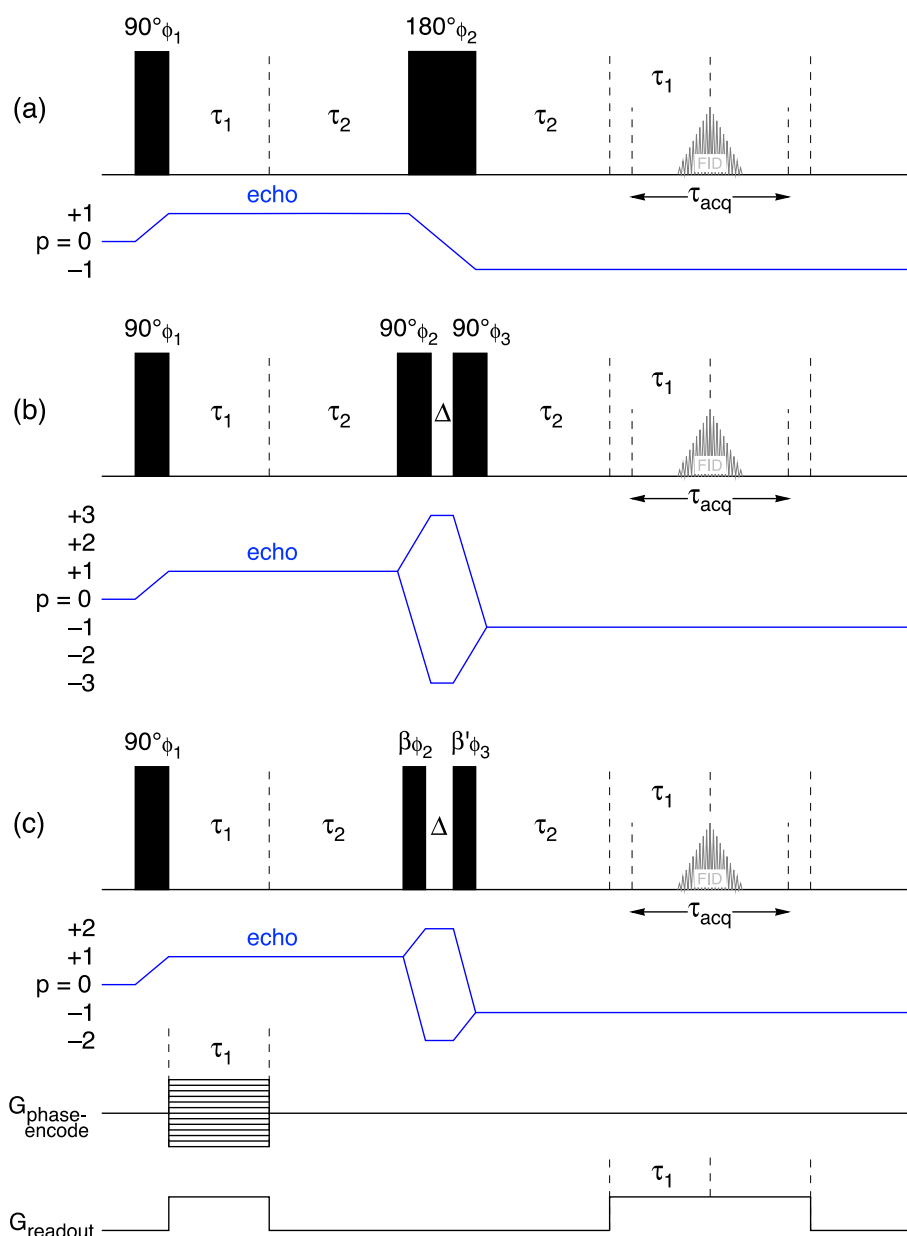
Fig. 2. Pulse and gradient sequences and coherence pathways for ^{23}Na ($I = 3/2$) MRI experiments used in this work. (a) Conventional spin-echo sequence. (b) A previously demonstrated triple-quantum filtered echo sequence [12,14]. (c) The double-quantum filtered echo sequence; correct choice of the flip angles β and β' allows selective detection of sodium ions that are interacting with ordered structures and so exhibit quadrupolar splittings in their ^{23}Na NMR spectrum. All three MRI experiments utilise the echo coherence pathway and so will achieve full refocusing of the effects of B_0 inhomogeneity if performed with the timings shown.
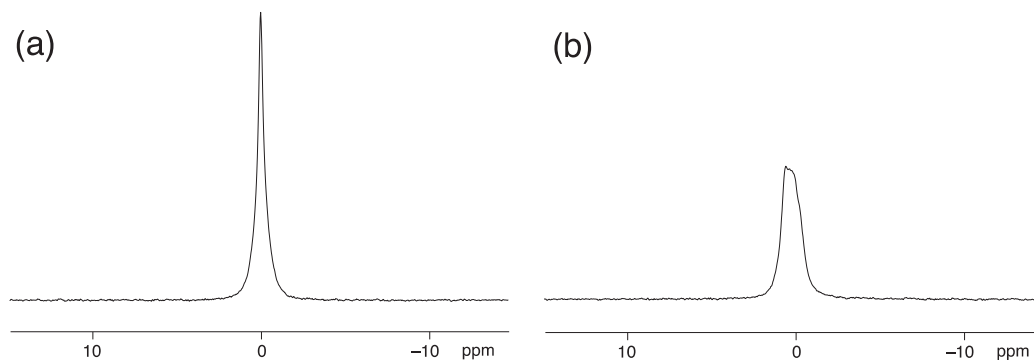
Fig. 3. The conventional ^{23}Na NMR spectrum of 3% (w/v) xanthan gum in 150 mM NaCl(aq). The number of transients averaged was 8. In (a) the B_0 field was shimmed to achieve an acceptable experimental ^{23}Na lineshape (full-width at half-height, 45 Hz). In (b) the z shim was deliberately misset, spoiling the B_0 inhomogeneity and hence broadening the ^{23}Na lineshape (full-width at half-height, 142 Hz). These two settings of the shims were used to represent nominally homogeneous and inhomogeneous B_0 fields in the NMR experimental work presented in Figs. 4 and 5.
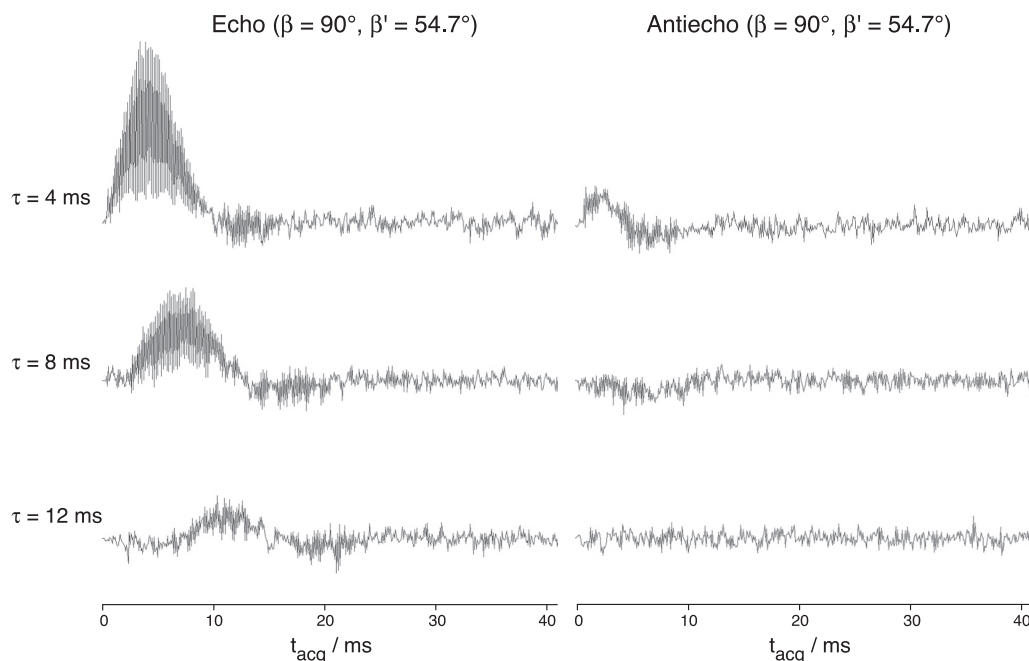
Fig. 4. ^{23}Na NMR of 3% (w/v) xanthan gum in 150 mM NaCl(aq). Free induction decays obtained from both the echo and antiecho versions of the double-quantum filter experiment in Fig. 1b in an inhomogeneous B_0 field, i.e., performed with the misset z shim as in Fig. 3b. Phase cycles for the echo and antiecho experiments are given in Table 1. The pulse flip angles in the double-quantum filter were set to $\beta = 90°$ and $\beta' = 54.7°$. The number of transients averaged was 64 and the 90° pulse duration calibrated as 128 μs. The free induction decays are shown for three values of the evolution period τ, as indicated. The presence of an echo signal at $t_{acq} = \tau$ is confirmed for the echo experiment.

mm tube of xanthan gum, plus two further elements. The first was 4% (w/v) agarose in 150 mM NaCl(aq) contained in a 10-mm glass NMR tube. Unlike xanthan gum, the agarose polymer produces an isotropic sodium ion environment and hence the ^{23}Na NMR spectrum is liquid-like, with no quadrupolar splittings and with no signal appearing in a "magic-angle" double-quantum filtered NMR experiment. However, the sodium ions in the agarose gel sample experience slow dynamics and hence exhibit biexponential spin relaxation, with the optimum evolution period τ in a triple-quantum filtered ^{3}Na NMR experiment, indicating the maximum in the build-up of $T_{3,\pm 1}$ coherences, determined to be 16 ms. The final element in the MRI phantom was 150 mM NaCl(aq) contained in a 5-mm glass NMR tube. Here, the sodium ions experience very fast dynamics and so exhibit monoexponential spin relaxation, with no ^{23}Na NMR signal passing through either a double- or triple-quantum filter.

4. Results and discussion

4.1. ^{23}Na (I = 3/2) NMR spectroscopy

Fig. 3 shows the conventional ^{23}Na NMR spectrum of the sample of 3% (w/v) xanthan gum in 150 mM NaCl(aq). For Fig. 3a, the B_0 field was shimmed to achieve an acceptable experimental ^{23}Na lineshape, while in Fig. 3b the z shim was deliberately misset, spoiling the B_0 homogeneity, with the results shown. These two settings of the shims were used to represent nominally homogeneous and inhomogeneous B_0 fields in the NMR experimental work below, although it should be noted that some degree of B_0 inhomogeneity is also present in the former case.

Fig. 4 shows the xanthan gum ^{23}Na free induction decays obtained from both the echo and antiecho versions of the double-quantum filter experiment in Fig. 1b in an inhomogeneous B_0 field, i.e., performed with the
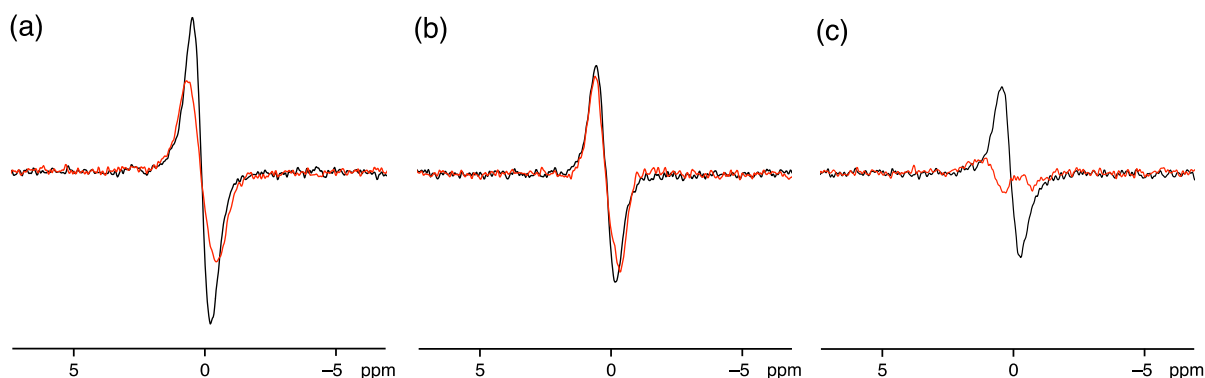
Fig. 5. Double-quantum filtered ^{23}Na NMR spectra of 3% (w/v) xanthan gum in 150 mM NaCl(aq) recorded in both homogeneous (black spectra) and inhomogeneous (red spectra) B_0 fields. The evolution period τ was 4 ms, the number of transients averaged was 64, and the 90° pulse duration calibrated as 128 μs. (a) Conventional double-quantum filtered spectra recorded using the pulse sequence in Fig. 1a (i.e., with a 180° pulse and two 54.7° pulses). The signal amplitude is reduced in the inhomogeneous B_0 field because no echo is formed in the acquisition period. (b) Double-quantum filtered echo spectra recorded using the pulse sequence in Fig. 1b (the blue coherence pathways with $\beta = 90°$ and $\beta' = 54.7°$). Here, as a result of the spin echo formed in the acquisition period at $t_{acq} = \tau$, the ^{23}Na NMR spectra have almost the same intensity in the homogeneous and inhomogeneous B_0 fields. (c) Double-quantum filtered antiecho spectra recorded using the pulse sequence in Fig. 1b (the red coherence pathways with $\beta = 90°$ and $\beta' = 54.7°$).

the misset z shim as in Fig. 3b. The pulse flip angles in the double-quantum filter were set to $\beta = 90°$ and $\beta' = 54.7°$ but fully equivalent results were obtained with $\beta = 54.7°$ and $\beta' = 90°$ (not shown). The free induction decays are presented for three values of the evolution period τ, as indicated. The presence of an echo signal at $t_{acq} = \tau$ is confirmed for the echo experiment, demonstrating that a spin echo can be formed by the two pulses of a multiple-quantum filter. In contrast, as expected, the antiecho experiment yields little signal in the inhomogeneous B_0 field and there is no evidence of a spin echo being formed.

Fig. 5 shows double-quantum filtered ^{23}Na NMR spectra of the xanthan gum sample recorded in both the homogeneous (black spectra) and inhomogeneous (red spectra) B_0 fields. The evolution period τ was 4 ms and 64 transients were averaged in each case.

In Fig. 5a, the conventional double-quantum filtration experiment in Fig. 1a (i.e., with a 180° pulse and two 54.7° pulses) has been used. As expected, a singly antiphase ^{23}Na NMR lineshape is obtained, arising solely from the spin I = 3/2 satellite transitions and indicative of $T_{2,-1}$ evolving into $T_{1,-1}$ during the acquisition period. However, the signal intensity is significantly lower in the inhomogeneous B_0 field than in the homogeneous one. This is because, although the 180° pulse removes the effects of B_0 inhomogeneity during the evolution period τ (by forming a spin echo at the end of that period), there is no spin echo formed during the acquisition period. At the time in the acquisition period when the maximum conversion of $T_{2,-1}$ into $T_{1,-1}$ has occurred (i.e., the peak of the quadrupolar echo), the signal will have undergone significant dephasing in the inhomogeneous B_0 field.

In Fig. 5b, the double-quantum filtered echo experiment (the blue coherence pathways in Fig. 1b) with $\beta = 90°$ and $\beta' = 54.7°$ has been used. Here, as a result of the spin echo formed in the acquisition period at $t_{acq} = \tau$, the ^{23}Na NMR spectra have almost the same intensity in the homogeneous and inhomogeneous B_0 fields. The small reduction in signal amplitude in the inhomogeneous field is simply the effect of the additional line broadening of the ^{23}Na lineshape caused by the B_0 inhomogeneity. Comparing Fig. 5a and b, it can be seen that, in the homogeneous B_0 field (black spectra), the signal amplitude is greater in the conventional "magic angle" double-quantum filtered spectrum (Fig. 5a). This is because the experiment used in Fig. 5a retains both coherence pathways in the evolution period, whereas the double-quantum filtered echo experiment used in Fig. 5b retains only the p = +1 pathway in the evolution period. However, in the inhomogeneous B_0 field (red spectra), the signal amplitude is greater in the double-quantum filtered echo spectrum (Fig. 5b).

In Fig. 5c, the double-quantum filtered antiecho experiment (the red coherence pathways in Fig. 1b) with $\beta = 90°$ and $\beta' = 54.7°$ has been used. As expected, this experiment performs relatively poorly in the nominally homogeneous B_0 field (because there is always some degree of B_0 inhomogeneity) and very poorly in the inhomogeneous B_0 field.

4.2. ^{23}Na (I = 3/2) MRI

Two-dimensional MRI experiments were performed using the pulse and gradient sequences shown in Fig. 2 (hence only one phase-encoding gradient was used) with Cartesian sampling of the time domain. Fig. 6a shows a ^{1}H spin-echo image of the xanthan + agarose + NaCl(aq) phantom recorded using the simple spin-echo sequence in Fig. 2a. We have labelled the three glass tubes comprising the phantom in the contour plot on the left. The "eye" shows the perspective used to generate the surface plot on the right. As is standard practice in a spin-echo image, in this and all the experiments shown in Fig. 2 we have ensured that the echo generated by the readout gradient is coincident in the acquisition period with that generated by the inherent B_0 inhomogeneity by using a constant amplitude for the readout gradient before and after the 180° pulse and by using the timings shown in Fig. 2.

Fig. 6b shows a ^{23}Na spin-echo image of the phantom recorded using the simple spin-echo sequence in Fig. 2a and the phase cycle given in Table 1. The image is similar to the ^{1}H image except that the 5-mm tube
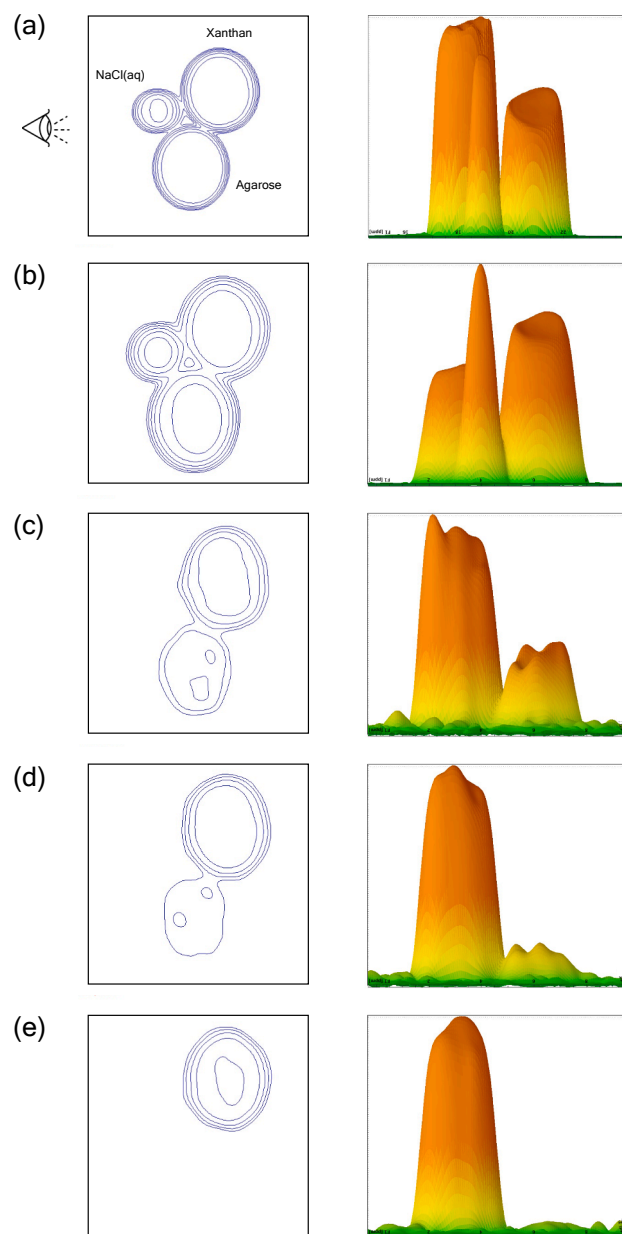

Fig. 6. Two-dimensional MRI of the xanthan + agarose + NaCl(aq) phantom described in the text, presented as contour plots (left) and surface plots (right); the "eye" shows the perspective used to generate the surface plots. (a) ^{1}H spin-echo image recorded with the pulse sequence in Fig. 2a (40 μs 90° pulse, 25 kHz spectral width, full field-of-view 39 × 39 mm², 64 complex points in $\tau_{acq} = 2.56$ ms, $\tau_1 = 1.28$ ms phase-encoding gradient, $\tau_1 + \tau_2 = 8.58$ ms evolution period, 1.0 s relaxation delay, 4 transients averaged for each of 64 phase-encoding steps, 4.3 min total imaging time, data zero-filled to 128 × 128, sine-squared weighting applied). (b) ^{23}Na spin-echo image recorded with the pulse sequence in Fig. 2a (125 μs 90° pulse, 25 kHz spectral width, full field-of-view 36 × 36 mm², 32 complex points in $\tau_{acq} = 1.28$ ms, $\tau_1 = 0.64$ ms phase-encoding gradient, $\tau_1 + \tau_2 = 5.0$ ms evolution period, 200 ms relaxation delay, 64 transients averaged for each of 32 phase-encoding steps, 7.2 min total imaging time, data zero-filled to 64 × 64, sine-squared weighting applied). (c) ^{23}Na triple-quantum filtered echo recorded with the pulse sequence in Fig. 2b (as in (b) except $\Delta = 2$ μs and 648 transients averaged for each of 32 phase-encoding steps, 73 min total imaging time). (d) ^{23}Na double-quantum filtered echo recorded with the pulse sequence in Fig. 2c and $\beta = \beta' = 54.7°$ (as in (c) except 640 transients averaged for each of 32 phase-encoding steps, 72 min total imaging time). (e) ^{23}Na double-quantum filtered echo recorded with the pulse sequence in Fig. 2c and $\beta = 90°$ and $\beta' = 54.7°$ (as in (d), 72 min total imaging time).

containing NaCl(aq) is now the most intense as a result of its ^{23}Na spin–spin (T_2) relaxation time being longer than that in the xanthan gum or agarose gel.

Fig. 6c shows a ^{23}Na triple-quantum filtered echo image [12,14] of the phantom recorded using the pulse sequence in Fig. 2b and the 18-step phase cycle given in Table 1 (which uses the 3-step phase cycle to select $\Delta p = -2$ over the two filter pulses [29]). As expected, the signal from the 5-mm tube containing NaCl(aq) is now absent, as spin I = 3/2 triple-quantum coherences cannot be excited in the monoexponentially relaxing sodium nuclei in the simple aqueous solution. For comparison across the four ^{23}Na images in Fig. 6b–e, we have recorded all the experiments with an evolution period of $\tau = \tau_1 + \tau_2 = 5$ ms. It should be noted that, although this is close to the optimum for the excitation of double-quantum coherences in our xanthan sample, it is less than the optimum for the excitation of triple-quantum coherences in both the xanthan and, in particular, agarose samples and this explains the rather indifferent signal-to-noise ratio in the image in Fig. 6c.

Fig. 6d shows a ^{23}Na double-quantum filtered echo image of the phantom recorded using the pulse sequence in Fig. 2c, the phase cycle given in Table 1, and flip angles $\beta = \beta' = 54.7°$. As predicted both in Eq. (18a) of Section 2.2 and by Gast et al. [27], this combination of flip angles fails to fully suppress the rank $l = 3$ coherences that have built up in the agarose sample due to spin I = 3/2 biexponential spin relaxation and the agarose tube still appears in the image with low intensity.

Finally, Fig. 6e shows the ^{23}Na double-quantum filtered echo image of the phantom recorded using the pulse sequence in Fig. 2c, the phase cycle given in Table 1, and flip angles $\beta = 90°$ and $\beta' = 54.7°$, as championed in this work. Both the 5-mm tube containing NaCl(aq) and the 10-mm tube containing agarose gel are now fully suppressed in the image, with only the tube containing xanthan gum appearing on account of its ^{23}Na NMR spectrum exhibiting quadrupolar splittings.

5. Conclusions

We have proposed and demonstrated a "magic angle" double-quantum filtered ^{23}Na NMR experiment that utilises just the echo coherence pathway during the evolution period and so achieves complete refocusing of the effects of B_0 inhomogeneity without making use of a 180° pulse. The new method has been demonstrated in ^{23}Na NMR spectroscopy in an inhomogeneous B_0 field where it achieved a greater signal-to-noise ratio than the conventional experiment that uses a 180° pulse (Fig. 5).

For the application of the new method to ^{23}Na MRI (Fig. 6), we have adopted an approach previously used in triple-quantum filtered ^{23}Na MRI where the phase-encoding gradients and the first segment of the readout gradient are applied before the multiple-quantum filter [12,14]. The evolution period τ in both double- and triple-quantum filtered ^{23}Na NMR must be of a certain duration (which should be calibrated or at least estimated), usually a few ms, to allow the function $g_{21}(\tau)$ or $f_{31}(\tau)$ to reach its maximum value and this essential, fixed-duration period can be used additionally for phase encoding. This allows the time after the multiple-quantum filter to be devoted entirely to acquiring the echo signal in the second part of the readout gradient. The triple-quantum filtered echo MRI sequence in Fig. 2b and the double-quantum filtered echo MRI sequence in Fig. 2c are entirely analogous to the simple spin-echo MRI sequence in Fig. 2a.

Methods for selectively imaging sodium ions in ordered environments have been around a long time [15] but their application to human studies [26,27] is clearly a field of research that is still in its infancy. The "magic angle" double-quantum filtered echo method proposed and demonstrated for ^{23}Na MRI in this work appears to offer an effective solution to the problem of imaging ordered sodium in an inhomogeneous B_0 field and it is hoped this will stimulate further endeavour in this area.

CRediT authorship contribution statement

Stephen Wimperis: Writing – review & editing, Writing – original draft, Visualization, Validation, Supervision, Software, Project administration, Methodology, Investigation, Formal analysis, Conceptualization. **Galina E. Pavlovskaya:** Resources, Investigation, Funding acquisition, Data curation.

Declaration of competing interest

The authors declare the following financial interests/personal relationships which may be considered as potential competing interests: Galina E. Pavlovskaya reports financial support was provided by UK Research and Innovation Medical Research Council. If there are other authors, they declare that they have no known competing financial interests or personal relationships that could have appeared to influence the work reported in this paper.

Acknowledgements

Data availability

Data will be made available on request.

References

[1] S. Vega, Y. Naor, Triple quantum NMR on spin systems with I = 3/2 in solids, J. Chem. Phys. 75 (1981) 75–86.
[2] J. Pekar, J.S. Leigh Jr., Detection of biexponential relaxation in sodium-23 facilitated by double-quantum filtering, J. Magn. Reson. 69 (1986) 582–584.
[3] G. Jaccard, S. Wimperis, G. Bodenhausen, Multiple-quantum NMR spectroscopy of S = 3/2 spins in isotropic phase: a new probe for multiexponential relaxation, J. Chem. Phys. 85 (1986) 6282–6293.
[4] L. Frydman, J.S. Harwood, Isotropic spectra of half-integer quadrupolar spins from bidimensional magic-angle spinning NMR, J. Am. Chem. Soc. 117 (1995) 5367–5368.
[5] T. Meersmann, S.A. Smith, G. Bodenhausen, Multiple-quantum filtered xenon- 131 NMR as a surface probe, Phys. Rev. Lett. 80 (1998) 1398–1401.
[6] C.W. Chung, S. Wimperis, Optimum detection of spin-3/2 biexponential relaxation using multiple-quantum filtration techniques, J. Magn. Reson. 88 (1990) 440–447.
[7] U. Eliav, H. Shinar, G. Navon, The formation of a second-rank tensor in ^{23}Na double-quantum-filtered NMR as an indicator for order in a biological tissue, J. Magn. Reson. 98 (1992) 223–229.
[8] R. Kemp-Harper, S.P. Brown, C.E. Hughes, P. Styles, S. Wimperis, ^{23}Na NMR methods for selective observation of sodium ions in ordered environments, Prog. NMR Spectrosc. 30 (1997) 157–181.
[9] R.H. Griffey, B.V. Griffey, N.A. Matwiyoff, Triple-quantum-coherence-filtered imaging of sodium ions in vivo at 4.7 tesla, Magn. Reson. Med. 13 (1990) 305–313.
[10] M.D. Cockman, L.W. Jelinski, J. Katz, D.J. Sorce, L.M. Boxt, P.J. Cannon, Double-quantum filtered sodium imaging, J. Magn. Reson. 90 (1990) 9–18.
[11] S. Wimperis, B. Wood, Triple-quantum sodium imaging, J. Magn. Reson. 95 (1991) 428–436.
[12] S. Wimperis, P. Cole, P. Styles, Triple-quantum filtration NMR imaging of 200 mM sodium at 1.9 tesla, J. Magn. Reson. 98 (1992) 628–636.
[13] J.R. Keltner, S.T.S. Wong, M.S. Roos, Three-dimensional triple-quantum-filtered imaging of 0.012 M and 0.024 M ^{23}Na using short repetition times, J. Magn. Reson. B 104 (1994) 219–229.
[14] R. Kemp-Harper, P. Styles, S. Wimperis, Three-dimensional triple-quantum filtration ^{23}Na NMR imaging, J. Magn. Reson. B 108 (1995) 280–284.
[15] C.E. Hughes, R. Kemp-Harper, P. Styles, S. Wimperis, NMR spectroscopy and imaging of sodium in ordered environments. The return of the central transition, J. Magn. Reson. B 111 (1996) 189–193.
[16] R. Kemp-Harper, P. Styles, S. Wimperis, B_1-selective pulses, J. Magn. Reson. A 123 (1996) 230–236.
[17] I. Hancu, F.E. Boada, G.X. Shen, Three-dimensional triple-quantum-filtered ^{23}Na imaging of in vivo human brain, Magn. Reson. Med. 42 (1999) 1146–1154.
[18] A. Borthakur, I. Hancu, F.E. Boada, G.X. Shen, E.M. Shapiro, R. Reddy, In vivo triple quantum filtered twisted projection sodium MRI of human articular cartilage, J. Magn. Reson. 141 (1999) 286–290.
[19] C. Tanase, F.E. Boada, Triple-quantum-filtered imaging of sodium in presence of B_0 inhomogeneities, J. Magn. Reson. 174 (2005) 270–278.
[20] C. Matthies, A.M. Nagel, L.R. Schad, P. Bachert, Reduction of B_0 inhomogeneity effects in triple-quantum-filtered sodium imaging, J. Magn. Reson. 202 (2010) 239–244.

[21] L. Fleysher, N. Oesingmann, M. Inglese, B_0 inhomogeneity-insensitive triple-quantum-filtered sodium imaging using a 12-step phase-cycling scheme, NMR Biomed. 23 (2010) 1191–1198.

[22] A. Tsang, R.W. Stobbe, C. Beaulieu, Triple-quantum-filtered sodium imaging of the human brain at 4.7 T, Magn. Reson. Med. 67 (2012) 1633–1643.

[23] D.P. Fiege, S. Romanzetti, D.H.Y. Tse, D. Brenner, A. Celik, J. Felder, N.J. Shah, B_0 insensitive multiple-quantum resolved sodium imaging using a phase-rotation scheme, J. Magn. Reson. 228 (2013) 32–36.

[24] C. Mirkes, G. Shajan, J. Bause, K. Buckenmaier, J. Hoffmann, K. Scheffler, Triple-quantum-filtered sodium imaging at 9.4 Tesla, Magn. Reson. Med. 75 (2016) 1278–1289.

[25] G.E. Pavlovskaya, T. Meersmann, Spatial mapping of flow-induced molecular alignment in a noncrystalline biopolymer fluid using double quantum filtered (DQF) ^{23}Na MRI, J. Phys. Chem. Lett. 5 (2014) 2632–2636.

[26] A. Tsang, R.W. Stobbe, C. Beaulieu, In vivo double quantum filtered sodium magnetic resonance imaging of human brain, Magn. Reson. Med. 73 (2015) 497–504.

[27] L.V. Gast, T. Gerhalter, B. Hensel, M. Uder, A.M. Nagel, Double quantum filtered ^{23}Na MRI with magic angle excitation of human skeletal muscle in the presence of B_0 and B_1 inhomogeneities, NMR Biomed. 31 (2018) e4010.

[28] M.A.U. Hoesl, L.R. Schad, S. Rapacchi, Efficient ^{23}Na triple-quantum signal imaging on clinical scanners: Cartesian imaging of single and triple-quantum ^{23}Na (CRISTINA), Magn. Reson. Med. 84 (2020) 2412–2428.

[29] G. Bodenhausen, H. Kogler, R.R. Ernst, Selection of coherence-transfer pathways in NMR pulse experiments, J. Magn. Reson. 58 (1984) 370–388.

[30] S.P. Brown, S. Wimperis, NMR measurement of spin-3/2 transverse relaxation in an inhomogeneous B_1 field, Chem. Phys. Lett. 224 (1994) 508–516.

[31] R. Kemp-Harper, P. Styles, S. Wimperis, Measurement of ^{23}Na transverse relaxation in vivo. The flip-angle-independent experiment, J. Magn. Reson. B 109 (1995) 223–228.

[32] L.V. Gast, T. Platt, A.M. Nagel, T. Gerhalter, Recent technical developments and clinical research applications of sodium (^{23}Na) MRI, Prog. NMR Spectrosc. 138–139 (2023) 1–51.

[33] N. Muller, G. Bodenhausen, R.R. Ernst, Relaxation induced violations of coherence transfer selection rules in nuclear magnetic resonance, J. Magn. Reson. 75 (1987) 297–334.

[34] S. Antonijevic, S. Wimperis, Refocussing of chemical and paramagnetic shift anisotropies in ^{2}H NMR using the quadrupolar-echo experiment, J. Magn. Reson. 164 (2003) 343–350.

[35] G. Bodenhausen, R. Freeman, D.L. Turner, Suppression of artifacts in two-dimensional J spectroscopy, J. Magn. Reson. 27 (1977) 511–514.